Title: BDNF signaling in Hebbian and Stentian structural plasticity in the developing visual system

Authors: Elena Kutsarova[1,2], Anne Schohl[1], Martin Munz[1,3,4] Alex Wang[1,5], Yuan Yuan Zhang[1,6], Olesia M Bilash[1,7], Edward S Ruthazer[1]*

Affiliations:1. Montreal Neurological Institute-Hospital, McGill University, Montreal, QC H3A 2B4, Canada

2. Max Planck Institute for Brain Research, 60438 Frankfurt, Germany

3. Institute of Molecular and Clinical Ophthalmology Basel, 4031 Basel, Switzerland

4. Department of Ophthalmology, University of Basel, 4056 Basel, Switzerland

5. Interdepartmental Neuroscience, Yale University, New Haven, CT

6. Faculty of Medicine, University of Ottawa, Ottawa, Canada

7. NYU Neuroscience Institute, New York University, New York, NY 10016

*to whom communication should be addressed: edward.ruthazer@mcgill.ca

Keywords: *Xenopus laevis*, retinotectal, TrkB, $p75^{NTR}$, retinal ganglion cell, axon, activity-dependent, *in vivo* imaging

Abstract

During development, patterned neural activity instructs topographic map refinement. Axons with similar patterns of neural activity, converge onto target neurons and stabilize their synapses with these postsynaptic partners, restricting exploratory branch elaboration (Hebbian plasticity). On the other hand, non-correlated firing in inputs leads to synapse weakening and increased exploratory growth of axons (Stentian plasticity). We used visual stimulation to control the correlation structure of neural activity in a few ipsilaterally projecting (ipsi) retinal ganglion cell axons with respect to the majority contralateral eye inputs in the optic tectum of albino *Xenopus laevis* tadpoles. Multiphoton live imaging of ipsi axons, combined with specific disruptions of brain-derived neurotrophic factor (BDNF) signaling, revealed that both presynaptic $p75^{NTR}$ and TrkB promoted Stentian axonal branch addition, whereas presumptive postsynaptic BDNF signaling mediated Hebbian axon stabilization. Additionally, we found that BDNF signaling contributes to suppression of branch elimination locally in response to correlated firing of inputs.

Introduction

Sensory experience during early development is crucial for the formation of precise topographic maps throughout the brain (López-Bendito and Molnár, 2003). Retinal ganglion cells (RGCs) in fish and amphibians can fire action potentials in response to visual stimuli during the period when they first extend into the optic tectum, whereas in mammalian development, spontaneous waves of retinal activity drive RGC patterned activity (Holt and Harris, 1983; Demas et al., 2012; Arroyo and Feller, 2016; Pratt et al., 2016). Therefore, temporal correlation in firing patterns of RGCs is indicative of their mutual proximity in the retina, and the developing visual system uses this information to instruct structural and functional refinement of retinotopic and higher-order feature maps (Zhang et al., 2011; Munz et al., 2014; Kutsarova et al., 2016). Concretely, co-activation of RGC inputs, read out by calcium flux through postsynaptic N-methyl-D-aspartate receptors (NMDARs), stabilizes retinotectal synapses and their axonal arbors (Cline et al., 1987; Rajan et al., 1999; Ruthazer et al., 2003; Mu and Poo, 2006; Munz et al., 2014; Kesner et al., 2020). This correlation-dependent stabilization is called “Hebbian plasticity” (Hebb, 1949). In contrast, asynchronous firing of RGC axons with respect to their neighboring inputs leads to synaptic weakening, accompanied by an increase in axonal branch dynamics and exploratory growth, referred to as “Stentian plasticity” (Stent, 1973; Munz et al., 2014). Evidence indicates that it is activity in neighboring axons that promotes the Stentian synaptic weakening and branch elaboration of those axons that have not been stabilized by correlated firing and NMDAR activation (Rahman et al., 2020). Brain-derived neurotrophic factor (BDNF) has been implicated as a potent modulator of synaptic and structural plasticity throughout the brain (Zagrebelsky and Korte, 2014). BDNF can be synthesized and released in a constitutive or activity-dependent manner from axonal terminals and dendrites (Mowla et al., 1999; Balkowiec and Katz, 2000; Yang et al., 2009; Dieni et al., 2012; Orefice et al., 2016; Vignoli et al., 2016). It can be released as an active precursor form, proBDNF, which exerts its function mainly via $p75^{NTR}$ and sortilin signaling, or as the cleaved mature form (mBDNF), which signals mainly via TrkB and $p75^{NTR}$/TrkB (Chao and Hempstead, 1995; Rösch et al., 2005; Woo et al., 2005; Baho et al., 2019). The specifics of BDNF synthesis, secretion and receptor signaling create multi-layered regulation underlying the diversity of

66 functions served by BDNF in the brain. Notably, at developing neuromuscular synapses,
67 proBDNF signaling through presynaptic $p75^{NTR}$ is required for axonal retraction, whereas
68 mBDNF signaling through presynaptic TrkB leads to axonal stabilization (Je et al., 2012,
69 2013). In the developing retinotectal system, exogenous application of BDNF induces
70 RGC axon branching and growth, whereas depletion of endogenous BDNF impedes
71 presynaptic synaptobrevin punctum formation and axonal branch stabilization (Cohen-
72 Cory and Fraser, 1995; Alsina et al., 2001; Hu et al., 2005; Marshak et al., 2007). BDNF
73 signaling through the TrkB receptor is necessary for Hebbian synaptic strengthening
74 induced by visual conditioning in the Xenopus retinotectal system, whereas proBNDF
75 signaling through $p75^{NTR}$ facilitates synaptic weakening (Mu and Poo, 2006; Schwartz et
76 al., 2011).
77 To test what aspects of BDNF signaling are respectively involved in Hebbian and
78 Stentian structural plasticity, we took advantage of ipsilaterally projecting (ipsi) RGC
79 axons in albino *Xenopus laevis* tadpoles, which typically consist of just one or two ectopic
80 axons and which spontaneously occur in fewer than half of all animals (Munz et al.,
81 2014). Exploiting the presence of an ipsi axon, we used optical fibers to present light to
82 each eye, visually stimulating the ipsi axon in or out of synchrony with the contralateral
83 eye from which the bulk of inputs originates. Furthermore, we selectively knocked down
84 either $p75^{NTR}$ or TrkB in these ipsi axons, demonstrating evidence by *in vivo* imaging for
85 the presynaptic involvement of these neurotrophin receptors as positive regulators of
86 Stentian axonal branching and growth. We further found that Hebbian stabilization was
87 blocked by application of an extracellular TrkB-Fc, which prevented BDNF signaling.
88

89 ## Results

90 ***Stentian and Hebbian structural plasticity are mediated by distinct components of***
91 ***BDNF signaling***

92 We performed *in vivo* 2-photon imaging of EGFP-expressing ipsi RGC axonal arbors
93 in the optic tectum every 10 min for up to 5 h while subjecting the animals to a Darkness-
94 Asynchronous-Synchronous (DAS) visual stimulation protocol (**Figures 1A and 1B**). Ipsi
95 RGC axons exhibit greater branch dynamics and growth when stimulated
96 asynchronously with respect to the majority contra RGC inputs, but synchronous

activation of the ipsi and contra axons results in arbor stabilization (Munz et al., 2014). To examine the importance of BDNF signaling, we employed two strategies: either intraventricular injection of TrkB-Fc to sequester released BDNF acutely, or co-electroporation of EGFP and antisense morpholino oligonucleotide (MO) against $p75^{NTR}$ or TrkB in the eye to achieve presynaptic knock-down of these receptors in the RGCs (**Figure 1A, Figure S1**). MOs were tagged with the red fluorescent dye lissamine which filled the entire the RGC out to its axonal terminal, permitting knock-down to be confirmed by the presence of both EGFP and lissamine fluorescence in individual ipsi axons. We quantified the numbers of newly added and lost branches per axon for each 10 min imaging interval throughout the DAS protocol (**Figures 1B and 1C**). Ipsi axons containing Ctrl-MO (Control) exhibited increased branch additions during asynchronous stimulation of the two eyes compared to synchronous stimulation (**Figures 1D and 1F**) in line with a previous report (Munz et al., 2014). In p75-MO and in TrkB-MO ipsi axons, the increase in branch additions induced by asynchronous stimulation was prevented (**Figures 1D and 1F**), indicating a direct role of neurotrophin receptor activation in Stentian plasticity.

On the other hand, the Hebbian suppression of new branch additions during synchronous binocular stimulation (Munz et al., 2014) was prevented by depletion of BDNF signaling by extracellular application of TrkB-Fc (**Figures 1D and 1F**). The significant increase in branch additions during synchronous stimulation exclusively in TrkB-Fc treated, but not in neurotrophin receptor knock-down RGC axons, suggests a key role for BDNF release or extracellular processing in Hebbian suppression of branch addition. Interestingly, we observed significantly higher rates of branch addition during synchronous stimulation in BDNF depleted tecta, compared to presynaptic $p75^{NTR}$ or TrkB knock-down, implying that BDNF acts on targets other than the axon itself, presumably the postsynaptic terminal, to induce Hebbian retrograde signals that inhibit formation of new axonal branches.

Presynaptic BDNF signaling helps suppress branch loss during stimulation

In the optic tectum, RGC axons, their postsynaptic partners, and surrounding glia, all rapidly extend and retract processes in the neuropil during structural refinement of the

128 developing retinotopic map. Axonal branch elimination occurs in parts of the arbor where
129 synapses have failed to undergo stabilization, permitting axon pruning and topographic
130 map refinement (Kutsarova et al., 2016). Knock-down of $p75^{NTR}$ or TrkB in the ipsi RGC
131 axon, as well as broad depletion of BDNF signaling, led to an overall increase in the
132 rates of axonal branch loss in response to visual stimulation compared to control ipsi
133 axons (**Figures 1E and 1G**). Thus, under normal conditions, BDNF signaling can help
134 stabilize axons against activity-induced axonal branch loss.
135
136 ***BDNF signaling spatially restricts branch elimination events***
137 Local action of BDNF has previously been shown to alter synaptic maturation and
138 dendritic morphology in cells in close proximity to release sites (Horch and Katz, 2002;
139 Zhang and Poo, 2002; Ohba et al., 2005; Kohara et al., 2007). We set out to further
140 explore the role of BDNF signaling in the spatial organization of axonal branch addition
141 and elimination events in response to patterned activity (**Figures 2A and 2B**). To assess
142 whether remodeling events occurred in close proximity to each other, indicative of local
143 signaling on the arbor, we extracted the pairwise distances for all addition and for all
144 elimination events during darkness, asynchronous and synchronous stimulation (**Figure**
145 **2C**) and calculated a mean event pair distance for each stimulation period (**Figure 2D**),
146 shown for the example axon (**Figure 2C**). Differences in arbor size and shape may
147 impact measurements of mean event pair-distance. We therefore performed Monte
148 Carlo simulations of the locations of events on the arbor (**Figure S2**) and used the
149 simulated mean event pair-distances to correct for differences in arbor morphology for
150 all analyses. The corrected mean pairwise distance between elimination events was
151 significantly lower during synchronous stimulation compared to darkness in control
152 axons, consistent with fewer branch elimination events occurring far apart from each
153 other during correlated firing induced by synchronous stimulation (**Figures 2D and 2E**).
154 These data reveal that correlated activity causes branch eliminations to become
155 restricted to a relatively smaller portion of the total arbor, likely through the local
156 stabilization of some branches. Extracellular depletion of BDNF with TrkB-Fc, or knock-
157 down of $p75^{NTR}$ or TrkB in ipsi axons, resulted in a redistribution of branch elimination
158 events, no longer favoring the event proximity normally seen with synchronous

159 stimulation (**Figure 2E**). Interestingly, this spatial phenomenon was limited to branch
160 elimination, as we observed no difference in mean pairwise distances of addition events
161 in control axons across the stimulation periods (**Figure 2F**). These findings point to a
162 model in which secreted neurotrophin appears to influence branch eliminations and
163 stabilization within spatially constrained local zones of action.
164

165 ***Axon arbor elaboration over days relies on p75^{NTR} expression in the RGCs***

166 We followed the elaboration of individual RGC axons over 4 days, by co-
167 electroporating EGFP together with either p75-MO or TrkB-MO to assess the roles
168 played by these receptors in arbor remodeling, this time focusing our attention on the
169 predominant contra RGC axons (**Figures 3A-C**). Interestingly, RGC axons knocked-
170 down for p75^{NTR} exhibited a decreased accumulation of branch tips compared to axons
171 with TrkB-MO (**Figures 3D and 3E**), suggesting that p75^{NTR} promotes axonal branch
172 elaboration. Furthermore, p75^{NTR} knock-down also resulted in a significant decrease in
173 the axon skeletal length compared to control axons (electroporated with Ctrl-MO) and
174 RGCs electroporated with TrkB-MO (**Figure 3F**), pointing to a major role for p75^{NTR} in
175 axonal arbor growth. In addition, binning terminal segments (**Figure 3D**) by length
176 revealed that as axonal arbors became more complex over 4 days, the proportion of
177 terminal segments categorized as short (1-5 μm) decreased in control and TrkB-MO
178 axons, whereas it remained unchanged in the p75-MO axons, consistent with their failure
179 to undergo progressive elaboration (**Figure 3G**). These data reveal that p75^{NTR} in the
180 RGCs helps both to promote new branch accumulation and the elongation of the short
181 filopodium-like branches over days, resulting in a more complex terminal arbor.
182

183 ***p75^{NTR} and TrkB in RGCs play opposing roles in axonal arbor span enlargement***

184 The retinotopic map occupies a 3D volume within the tectum (Li et al., 2022), and
185 therefore a relevant metric of an axon's morphology and refinement is the volume of its
186 arbor span. We calculated arbor span volume by obtaining a measure of the convexity
187 of the 3D reconstructed axonal arbor, which was used to define an enclosing volume
188 whose border lies between a tight fit and a convex hull around the arbor, as described
189 by Bird and Cuntz (2019) (**Figures 4A-C**). We found that knock-down of p75^{NTR} and TrkB

190 in RGCs resulted in opposite changes in arbor span volume, with TrkB-MO arbors
191 expanding more rapidly over 4 days to occupy a greater volume in the optic tectum
192 compared to p75-MO axons (**Figure 4D-E**). These observations suggest that $p75^{NTR}$ in
193 the RGC promotes enlargement of the axonal arbor span volume, whereas TrkB
194 impedes the expansion of RGC arbor volume.
195

196 ## Discussion

197 ***Presynaptic $p75^{NTR}$ and TrkB in Stentian exploratory growth***

198 We have shown that presynaptic knock-down of $p75^{NTR}$ and TrkB receptors blocks
199 the Stentian increase in new branch addition that occurs when an axon does not fire in
200 synchrony with its neighbors (**Figures 1D and 1F**) (Munz et al., 2014; Rahman et al.,
201 2020). Furthermore, we found a decrease in branch tip accumulation over 4 days of
202 repeated imaging in p75-MO axons (**Figure 3E**). Our finding that $p75^{NTR}$ promotes the
203 elongation of axonal branches specifically through the extension of the shortest
204 filopodium-like branches (**Figure 3G**) further clarifies the role of $p75^{NTR}$ in RGC axonal
205 exploratory growth. Previous work demonstrated that when inputs surrounding an axon
206 actively fire while that axon is quiescent, Stentian "exploratory growth" of the inactive
207 axon takes place, suggesting the possible release of an intercellular growth-promoting
208 signal by neighboring cells in the optic tectum (Rahman et al., 2020). From experiments
209 where we electroporated p75-MO exclusively in the ipsi eye, we can conclude that
210 $p75^{NTR}$ specifically on the asynchronously firing RGC axon mediates the response to
211 Stentian signals that promote branch addition and extension. Putative $p75^{NTR}$ ligands
212 could be released directly by the neighboring axons, indirectly by the postsynaptic
213 neurons or even by local glia. Further investigation is required to reveal the identities and
214 the exact sites of release of these potential ligands. However, proBDNF-induced
215 activation of $p75^{NTR}$ has been shown to promote synaptic weakening both in *Xenopus*
216 tadpoles and in mice (Woo et al., 2005; Schwartz et al., 2011; Winnubst et al., 2015),
217 consistent with prior reports that exploratory axon growth is accompanied by a marked
218 reduction in synaptic strength (Munz et al., 2014). Injection of BDNF in the optic tectum
219 drives a robust increase in RGC axonal branch number, an effect which could potentially
220 be the result of activation of either TrkB or $p75^{NTR}$ (Cohen-Cory and Fraser, 1995). The

221 molecular mechanisms following p75^{NTR} activation may differ in the somato-dendritic and
222 the axonal compartments due to differential expression of p75^{NTR} interacting partners (
223 Hermey et al., 2001; Wang et al., 2002; Bronfman and Fainzilber, 2004;). Activation of
224 dendritic p75^{NTR} has been shown to result in a reduction in dendritic branch complexity
225 and dendritic spine density in rodent hippocampal neurons (Yang et al., 2014; Orefice et
226 al., 2016). In contrast, our data demonstrate that *Xenopus* retinotectal axons exhibit
227 Stentian exploratory growth in response to p75^{NTR} activity.
228 In our daily imaging data, knock-down of TrkB exerted very little effect on contra axon
229 branch accumulation and elongation over days (**Figure 3**). One must consider, however,
230 that even during their early development, RGC axons exhibit coarse topographic order
231 within the optic tectum and thus, on average exhibit a pattern of firing that is relatively
232 correlated with that of their neighbors (McLaughlin et al., 2003). It is therefore plausible
233 that the level of correlated neural activity among contra axons obscures the effects of
234 Stentian plasticity for all but the most imprecisely targeted stray axons over days. The
235 short-term dynamic imaging of ipsi axons, which allowed us to systematically alter the
236 degree of correlation in RGC firing, unmasked a role for presynaptic TrkB in contributing
237 to Stentian structural plasticity through an increase in the rate of new branch addition
238 (**Figures 1D and 1F**).
239
240 ***BDNF signaling in Hebbian suppression of axonal branch addition***
241 The axonal branch stabilization induced by correlated firing is dependent on the
242 activation of NMDARs (Ruthazer et al., 2003; Munz et al., 2014). Specifically,
243 postsynaptic knock-down of NMDARs in optic tectal neurons results in an increased
244 number of branch tips in RGC axons, suggesting the existence of a putative retrograde
245 signal that promotes presynaptic axon arbor stabilization (Kesner et al., 2020). In
246 addition, such retrograde signaling appears to depend on the activation of CaMKII in the
247 optic tectal neurons (Zou and Cline, 1996). Sequestering extracellular BDNF prevented
248 the decrease in branch additions during synchronous stimulation in our experiments
249 involving dynamic imaging of ipsi axons, a result that was not replicated by axonal p75-
250 MO or TrkB-MO, suggesting that BDNF indirectly mediates axonal stabilization, perhaps
251 by acting postsynaptically to drive release of a putative retrograde signal (**Figures 1D**

252 **and 1F**). It is also plausible that BDNF may be released downstream of postsynaptic
253 NMDAR activation and act as an autocrine signal mediating synaptic strengthening
254 (Schwartz et al., 2011; Harward et al., 2016; Vignoli et al., 2016).
255 Our data provide evidence for BDNF acting both presynaptically to promote Stentian
256 exploratory branching and postsynaptically to drive Hebbian stabilization that results in
257 suppression of new branch addition. These opposing effects could reflect differences in
258 the levels of expression of TrkB and $p75^{NTR}$ and their interactors in dendrites and axons
259 as previously mentioned (Dougherty and Milner, 1999; Hermey et al., 2001; Wang et al.,
260 2002; Bronfman and Fainzilber, 2004). Another possibility is that proBDNF may be
261 released in response to neural activity to act on $p75^{NTR}$, but can be further converted to
262 mBDNF through NMDAR-dependent activation or release of tissue plasminogen
263 activator (tPA) or matrix metaloproteinase-9 (MMP-9), leading to preferential activation
264 of TrkB during synchronous stimulation (Qian et al., 1993; Pang et al., 2004;
265 Dziembowska et al., 2012). Moreover, tPA has been implicated in synaptic strengthening
266 in the retinotectal projection in response to visual conditioning (Schwartz et al., 2011).
267 There is evidence to suggest that MMP-9 is involved in the processing of proBDNF to
268 mBDNF leading to stabilization of a robustly firing motor axon in the NMJ, or in
269 strengthening of co-active synapses in the CNS (Je et al., 2012; Niculescu et al., 2018).
270 In the *Xenopus* optic tectum, MMP-9 is necessary for the visual experience driven
271 increase in tectal neuron dendritic growth (Gore *et al.*, 2021). Results from computational
272 modeling suggest that the ratio of proBDNF/mBDNF, regulated by local action of MMP-
273 9, combined with a precisely-timed rise in postsynaptic calcium may be crucial to switch
274 plasticity from depression to potentiation, presumably due to preferential activation of
275 $p75^{NTR}$ and TrkB, respectively (Kirchner and Gjorgjieva, 2021). It is also plausible that
276 the mode of BDNF release varies during asynchronous and synchronous stimulation, in
277 line with reports proposing that tonic versus acute release of BDNF may differentially
278 regulate the cell surface level of TrkB and thus distinctly affect neurite outgrowth
279 (Haapasalo et al., 2002; Ji et al., 2010; Guo et al., 2018).
280
281 ***Local action of BDNF signaling in Hebbian branch stabilization***

282 Our analyses on the spatial distributions of addition and elimination of axonal
283 branches revealed that correlated firing led to more locally targeted elimination events
284 compared to what occurs in darkness, whereas the mean distance between addition
285 events stayed similar regardless of stimulation (**Figures 2D-F**). These data are
286 consistent with previous observations in tadpoles with binocularly innervated optic tecta
287 showing that axonal branches are added uniformly across the arbor, but branch loss
288 tends to occur in the territory where inputs from the opposite eye dominate (Ruthazer et
289 al., 2003). Targeted axonal branch loss within restricted parts of the arbor is consistent
290 with the existence of widespread elimination-inducing signals counteracted by locally
291 diffusible signals that protect axonal branches from being eliminated in certain parts of
292 the arbor. We found that disrupting BDNF signaling in the retinotectal system resulted in
293 increased rates of branch elimination (**Figure 1E and 1G**). Our data suggest that local
294 release of BDNF locally confers axonal branch stabilization, such that blocking BDNF
295 signaling increases the probability of randomly occurring elimination events, even under
296 conditions of correlated neural activity. Altering the spatial distribution of elimination
297 events over longer time periods should lead to less compact arbors. Indeed, we observed
298 that TrkB knock-down in RGCs led to a notably enlarged axonal arbor span (**Figure 4**).
299 This effect on arbor span was not seen in $p75^{NTR}$ knock-down axons, most likely due to
300 their overall reduced arbor length and branch number.
301 In summary, the visual stimulation paradigm in these experiments revealed that
302 distinct aspects of BDNF signaling are responsible for Stentian and Hebbian structural
303 plasticity during development (**Figures 4F-H**). We propose that presynaptic $p75^{NTR}$ and
304 TrkB signaling promote aspects of Stentian exploratory growth (**Figure 4G**) in response
305 to asynchronous activity. In addition, BDNF, most likely acting postsynaptically, is
306 necessary for Hebbian suppression of new branch addition and acts locally within the
307 arbor to regulate axonal branch loss that occurs during correlated firing (**Figure 4H**).

Acknowledgements

We thank Kurt Haas (UBC) for Dynamo software, Kelly Sakaki (UBC) for ideas on imaging setup, Peter Donhauser (ESI) for discussions on image and statistical analysis, Tasnia Rahman (McGill) and Philip Kesner (McGill) for experimental blinding.

Funding

Funding sources are Jeanne Timmins Costello and Molson Neuroengineering Studentships (E.K.), Ann and Richard Sievers Award in Neuroscience (M.M.), McGill SURA (A.W.), CIHR Foundation Grant (FDN-143238; E.S.R.) and NSERC CREATE Neuroengineering Training Grant (E.S.R).

Author Contributions

E.K., A.S., MM. and E.S.R. conceived the experiments. E.K. and A.S. developed the methodology and generated resources. E.K., A.S., M.M., Y.Y.Z., A.W., O.M.B performed experiments. E.K. analyzed the data. E.K. and E.S.R. drafted the manuscript. All authors provided critical feedback and editing of the final manuscript. E.S.R. secured funding and supervised the project. For correspondence edward.ruthazer@mcgill.ca.

Conflict of interest

The authors declare no competing interests.

Materials and Methods

Accessibility

Any reagents generated for this study will be made available upon request to the lead contact. Alternatively, the requestor will be directed to a public repository tasked with distributing the reagent.

Raw axon reconstructions from which the analyses were performed will be uploaded to a public repository prior to final acceptance of the paper. These data are currently available at https://box.bic.mni.mcgill.ca/s/tbzd6t8N2Df1WV9

338 Custom MATLAB software (CANDLE denoising) used in this study is available for free
339 download at https://sites.google.com/site/pierrickcoupe/softwares/denoising-for-medical-
340 imaging/multiphoton-filtering. The analysis code is available at
341 https://github.com/ekutsarova/Dynamic-arbor-morphology-analysis.
342

343 ## *Xenopus laevis* tadpoles

344 The experiments described in this study were approved by the Animal Care Committee
345 at the Montreal Neurological Institute and are in accordance with the guidelines of the
346 Canadian Council on Animal Care. Animals of both sexes were used for the experiments;
347 At the stages of interest for our study, the sexes cannot be distinguished anatomically.
348 Albino *Xenopus laevis* tadpoles were generated by induced mating of a sexually mature
349 female frog, injected with pregnant mare serum gonadotropin (50 IU) 3 days before
350 mating and with 400 IU human chorionic gonadotropin (HCG) immediately before mating,
351 and a sexually mature male frog injected with 150 IU HCG up to 8 hours before mating.
352 The produced fertilized eggs were reared in 0.1X modified Barth's saline with HEPES
353 (MBSH).

354 ## Morpholino Oligonucleotides

355 *Xenopus* p75^{NTR} morpholino sequence: 5′-CCA TGC TGA TCC TAG AAA GCT GAT G-
356 3′ , referred to as p75-MO, *Xenopus* TrkB morpholino sequence: 5′-CCA CTG GAT CCC
357 CCC TAG AAT GGA G-3′ (Du and Poo, 2004; Je et al., 2012), referred to as TrkB-MO,
358 and standard control: 5'-CCT CTT ACC TCA GTT ACA ATT TAT A 3' (Gene Tools, LLC),
359 referred to as Ctrl-MO, were generated and tagged with lissamine on the 3'-end (Gene
360 Tools, LLC).
361

362 ## TrkB-MO validation experiments

363 Albino *Xenopus laevis* embryos were microinjected at the 2-cell stage with 18 ng of
364 Morpholino (TrkB-MO or Ctrl-MO) in each blastomere, using an automatic pressure
365 microinjector (Harvard Apparatus) with micropipettes pulled from glass (6.66 μL,
366 Drummond Scientific), using a Flaming Brown Micropipette Puller (P-97, Sutter
367 Instruments CO.). The morphant tadpoles were screened for lissamine fluorescence at
368 st. 46 (Nieuwkoop and Faber, 1994). Aside from one phospho-Trk antibody (Cell

369 Signalling, 9141, AB_2298805), the antibodies against TrkB that we tested showed lack
370 of specificity to the *Xenopus laevis* TrkB. We therefore validated the TrkB-MO by
371 measuring the level of phospho-TrkB in response to BDNF treatment between animals
372 injected with Ctrl-MO and TrkB-MO using the phospho-Trk antibody.
373 Stage 46 *Xenopus laevis* tadpoles injected at the 2-cell stage with TrkB-MO or Ctrl-MO
374 and positive for lissamine fluorescence were injected intraventricularly with 100 ng/µL
375 BDNF (B-250, Alomone Labs) using the same setup described for electroporation-related
376 DNA injections. After 1 h, brains were dissected and extracted in NP-40 extraction buffer
377 (10 mM HEPES/NaOH pH 7.4, 150 mM NaCl, 2 mM EDTA pH 8.0, 1% NP40) with Halt™
378 protease/phosphatase inhibitor cocktail (ThermoScientific, P178442). Brain extracts were
379 then homogenized using 10 s continuous 10% Amplitude on a Branson 250 Sonifier
380 (Branson Ultrasonics™) equipped with a microtip. The extracts were centrifuged at
381 13,000 rpm at 4°C for 10 min using a Biofuge 13 centrifuge (Heraeus Instruments).
382 Laemmli sample buffer (50 mM Tris/HCl pH 6.8, 10% Glycerol, 2% SDS, 0.025%
383 Bromphenol Blue, 100 mM DTT) was added to the supernatant and the protein samples
384 were then boiled at 100°C for 5 min for reduction and denaturation of the protein structure.
385 Proteins were separated on SDS-PAGE (8%) transferred to PVDF membranes
386 (Immobilon-P, 0.45 µm, Millipore) using wet transfer in transfer buffer (48 mM Tris base,
387 39 mM glycine, 0.037% SDS, 20% methanol). Molecular markers of known size
388 (Precision Plus Protein™ Dual Color Standard, Bio-Rad) were run in parallel with the
389 proteins of interest. Blots were probed with 1:5,000 rabbit anti-p-Trk (Cell Signalling,
390 9141, AB_2298805), 1:10,000 peroxidase AffiniPure Goat AntiRabbit IgG (H+L; Jackson
391 Immuno Research Laboratories, inc., 111-035-144, AB_2307391) was used for
392 visualization. Blots were blocked using 5% BSA (Fraction V, Fisher Scientific) in TBS-T
393 (20 mM Tris/HCl pH 7.6, 135 mM NaCl, 0.05% Tween) for p-Trk, and with 5% fat-free
394 milk in TBS-T for β-tubulin. To ensure equal loading the blots were probed with 1:20,000
395 rabbit anti-β-tubulin (sc-9104, Santa Cruz Biotechnology, AB_2241191) and 1:20,000
396 peroxidase AffiniPure Goat AntiRabbit IgG. Immobilon™ Western Chemiluminescent
397 HRP Substrate (Millipore) was used to visualize the protein bands on the blots, diluted
398 1:1 in double distilled water. HyBlot Autoradiography films (Denville Scientific, Inc.) were
399 used to collect images of the protein bands.

400

401 **p75-MO validation experiments**

402 Due to a lack of *Xenopus laevis* p75^{NTR}-specific antibody, we took an indirect route to
403 validate that the p75-MO knocks down *Xenopus laevis* p75^{NTR}. The p75^{NTR} sequence was
404 cloned from cDNA from st. 24 *Xenopus laevis* tadpoles (Nieuwkoop and Faber, 1994)
405 Total RNA was extracted from st. 24 tadpoles and cDNA was transcribed with Superscript
406 IV (Thermo Fisher, 18090010). The coding sequence (cds) of p75^{NTR} (starting from the
407 ATG, insensitive to the morpholino, MOres-p75^{NTR}) and the cds with part of the 5'UTR
408 (nucleotide -29 from ATG, sensitive to the morpholino, p75^{NTR}) were PCR amplified using
409 the following forward primers: MOres-p75^{NTR}: 5' ACG TGA ATT CAT GGA AAC CCC TCT
410 G 3', p75NTR: 5' ACG TGA ATT CCC TCA GCC ATC AGC T 3'. The reverse primer was
411 the same for both sequences, p75^{NTR}-reverse: 5' ACG TAC CGG TAA CAC GGG TGA
412 GGT A 3'. The PCR fragments were cloned in frame with EGFP into pCS2+ vector,
413 resulting in MOres-p75-EGFP and p75-EGFP. The plasmids were linearized with NotI
414 and mRNA was prepared with the SP6 mMessageMachine kit (Thermo Fisher, AM1340).
415 Animals were injected at the early 2-cell stage with 2 x 200 pg of either MOres-p75-EGFP
416 or p75-EGFP followed by injection of 2 x 18ng of p75-MO. Animals were screened for MO
417 (lissamine) and EGFP expression. In the animals expressing p75-EGFP and p75-MO
418 there was hardly any EGFP visible and lissamine was used to select animals. Whole
419 animals were extracted at st. 26 in NP40 extraction Buffer supplemented with Halt™
420 protease/phosphatase inhibitor cocktail (ThermoScientific, P178442). Samples were
421 incubated with Laemmli Buffer for 20 min at 37˚C. Extracts were separated on 8% SDS-
422 PAGE (as described in TrkB-MO validations experiments), transferred to PVDF
423 membrane and subsequently stained for EGFP (anti-GFP antibody, 1:20000, abcam
424 ab13970, AB_300798) and goat anti-chicken HRP 1:10,000 (Jackson Immuno Research
425 Laboratories, inc., 103-035-155, AB_233738) and β-tubulin (anti-β-tubulin, 1:20,000,
426 Santa Cruz sc-9104, AB_2241191) and AffiniPure Goat AntiRabbit IgG 1:20,000, as a
427 loading control. Blots were imaged on a BioRad ChemiDoc Imaging System.

428 Sparse labeling of contralaterally or ipsilaterally projecting RGC axons

429 Albino *Xenopus laevis* tadpoles (stages 40-42) were anaesthetized by immersion in
430 0.02% MS-222 (Sigma, A5040) diluted in 0.1X MBSH. The developmental stages were

431 determined using the standard criteria of Nieuwkoop and Faber (1994). EGFP DNA
432 plasmid (pEGFP-N1, Clonetech, 6085-1) and oligonucleotides were pressure-injected
433 into the eye using micropipettes pulled from borosilicate glass with filament (outer
434 diameter 1.0 mm, inner diameter 0.78 mm; Sutter Instruments) on a PC-10 puller
435 (Narishige, Japan) and attached to a custom-built manual pressure injection system.
436 Upon pressure injection of plasmid/morpholino solutions into the eye, current was
437 delivered across two custom-made platinum plates placed in parallel. A Grass 9 constant
438 voltage stimulator with a 3 μF capacitor placed in parallel was used to deliver 2 pulses in
439 each direction: 1.6 ms duration, 36 V for contra axons, 2.5 - 3 ms, 36 V for ipsi axons.
440 After electroporation, the animals were placed in a 20ºC biological oxygen demand
441 incubator in a 12h light/12h dark cycle. For long-term daily imaging of contra RGC axons,
442 RGCs were co-electroporated with MO and plasmid encoding EGFP (4.5 μg/μL : 1.5
443 μg/μL). To express EGFP in ipsi RGC axons, 2 μg/μL plasmid was pressure-injected. For
444 experiments involving ipsi knock-down of the BDNF receptors solution containing 3 μg/μL
445 : 4 μg/μL MO and EGFP was injected into the eye in order to achieve efficient co-delivery
446

447 **Daily imaging of morpholino-loaded/EGFP expressing RGC axons**

448 Animals at st. 45-46 (3 days post-electroporation) containing a single co-labeled RGC
449 axon were selected and imaged over the next 4 days. After anaesthetizing the tadpoles
450 by immersion in 0.02% MS-222 (Sigma, T2379) in 0.1x MBSH, they were positioned in
451 custom-made polydimethylsiloxane (PDMS) imaging chambers. Optical section z-series
452 at 1 μm steps of the axons of interest were acquired using an Olympus FV300 confocal
453 microscope converted for multiphoton use, equipped with a 60x LUMPlanFL N 1.0NA
454 water immersion objective. For optimal excitation of the axon-filling EGFP, imaging was
455 carried out at 910 nm once every day for 4 days. To confirm the presence of lissamine-
456 tagged MO in the axons of interest and assure minimal cross-talk between the two
457 channels (green: 500-550 nm and red: 593-668 nm) 3D fluorescence stacks were also
458 acquired at 840 nm where the EGFP excitation is minimal and the lissamine excitation
459 peaks.
460 Dynamic imaging of ipsilaterally projecting RGC axons combined with visual stimulation

461 Animals were given at least 4 days post-electroporation to assure labeling and proper
462 knock-down in ipsi axons and imaging was performed in stage 47-48 tadpoles. The
463 animals were immobilized by intraperitoneal injection of 2.5 mM tubocurarine
464 hydrochloride pentahydrate (Sigma). In the experiments including acute pharmacological
465 blockade, 50 µg/mL TrkB-Fc (Recombinant Human Chimera, 688-TK, R&D Systems) was
466 injected intraventricularly. The animals were then placed in a custom-built imaging
467 chamber (PDMS), fixed in place with a small drop of 1.8% UltraPureTM Low Melting Point
468 Agarose (Invitrogen, 16520). The imaging chamber contains two channels for fiber optics,
469 one leading to each eye, a perfusion and spillover chambers, as previously described
470 (Rahman et al., 2020). During the whole imaging session, the tadpoles were perfused
471 with O_2-bubbled 0.1x MBSH. Light flashes were delivered separately to each eye using
472 an FG365LEC-Custom optic fiber (ThorLabs) placed in a channel leading to each eye.
473 To generate light flashes Red Rebel 102lm@700mA LEDs (Luxeon Star, Ltd) controlled
474 by STG4002 and MC Stimulus-II software (Multichannel Systems) were used. After
475 stabilizing the tadpoles, the chamber was placed under the two-photon microscope where
476 the animals habituated in darkness for 30 min. Optical section z-series at 1 µm steps of
477 the EGFP-labeled ipsi axons were acquired every 10 min for 1 h in darkness followed by
478 1.5 h of asynchronous stimulation: 10 ms flashes, alternating between the two eyes at a
479 duty cycle of 0.5 Hz for each eye, followed by 1.5 h of synchronous stimulation:
480 simultaneous 10 ms flashes light in the two eyes presented at 0.5 Hz. For some
481 experiments involving knock-down of proteins of interest, optical section z-series of EGFP
482 and lissamine co-labeled RGC axons were acquired for 1 h in darkness, 2 h in
483 asynchronous and 2 h in synchronous stimulation. Imaging was performed at 910 nm
484 allowing optimal excitation of EGFP using a ThorLabs multiphoton microscope equipped
485 with XLUMPlanFL N 1.0 NA 20x WI objective (Olympus), two channels with gallium
486 arsenide phosphide photo-multiplier tubes (GaAsP PMTs) filtered to detect green and red
487 emission (525/50 and 630/92) and ThorImage software. For some experiments including
488 co-electroporation of EGFP and MO, additional optical section z-series were collected at
489 the end of each imaging session at 840 nm to ensure minimal excitation of EGFP and
490 maximal excitation of lissamine.
491

492 **Image Analysis**

493 All multiphoton z-series were denoised using CANDLE software implemented in MATLAB
494 (MathWorks) which relies on non-local mean filtering methods (Coupé et al., 2012).
495 Denoised 3D stacks were then used to reconstruct axonal arbors using “Autopath” and
496 “Autodepth” features in Imaris 6.4.2 (Bitplane) for daily imaging experiments and by
497 manual tracing in Dynamo software (Munz et al., 2014), implemented in MATLAB
498 (MathWorks), generously provided by Drs. Kaspar Podgorski and Kurt Haas (UBC). For
499 morphometric analysis of daily imaged RGC axonal terminal branch points were extracted
500 from Imaris 6.4.2. PyImarisSWC Xtension, implemented in Python, installed in Imaris
501 9.5.1, was used to export the Imaris reconstructions as swc-files. The exported node
502 coordinates were converted from pixel to µm. The swc-files were imported using “trees
503 toolbox” (Cuntz et al., 2010), which was used to classify axonal segments according to
504 their order derived by the Strahler ordering method, using “strahler_tree” function
505 (Strahler, 1957; Uylings et al., 1975; Vormberg et al., 2017). Axonal segments are defined
506 as axonal structure bordered by two branch points or by a branch and a terminal point.
507 The length of axonal segments with Strahler number of one, referred to as terminal
508 segments was extracted and the distribution of terminal segments binned by length was
509 followed over 4 days. The length of all segments with Strahler number>1 was counted
510 toward the total skeleton length. Axonal span volume was calculated after obtaining the
511 convexity of the 3D reconstructed arbors with “convexity_tree” function and then using
512 the value to calculate and feed a shrink factor into “boundary_tree” function of “tree
513 toolbox” as described by (Bird and Cuntz, 2019). From the dynamic imaging experiments
514 ipsi RGC axon branch additions and eliminations between two consecutive time-series
515 (10 min) were extracted and further normalizations were performed as described in each
516 individual case in the figure legends. A branch was counted towards any further analysis
517 only if it attained a length of 1.5 µm at some point during the imaging session. In two
518 axons the asynchronous stimulation was 10 min longer, and this extra timepoint was not
519 used for further analyses. In two axons a timepoint was missing resulting longer (20 min)
520 interval between two timepoints. Addition events were defined as the branch points of
521 newly added branches between “t-10 min” and “t”. Elimination events were defined as the
522 terminal points of branches lost between “t” and “t+10 min”. Rigid body transformation

523 using manual landmarks in Dynamo was applied to align the timepoints of the
524 reconstructed arbor. The coordinates of all the events throughout a stimulation period –
525 dark, asynchronous or synchronous, were extracted and the pairwise distances between
526 all the elimination and all the addition events were calculated. For one axon from the
527 TrkB-Fc group, there was only one elimination event throughout the dark period, which
528 prevented the calculation of mean elimination event pair distance for the dark period and
529 further normalization. Thus, this cell was excluded from the elimination event analyses.
530 To assess whether the changes in mean distances were explained by changes in axon
531 arbor morphology, a randomization of the events on the axonal arbor was performed. To
532 do that, the reconstructions in Dynamo were used to extract the coordinates of each node
533 and a swc-file was exported for each timepoint of the imaging session. The reconstruction
534 was then resampled using "resample_tree" from "trees_toolbox" such that the nodes
535 composing the arbor were equidistant at 0.15 µm. The number of observed addition
536 events between "t-10 min" and "t" was randomly distributed on the axonal arbor at "t". The
537 number of observed elimination events between t" and "t+10 min" was randomly assigned
538 to the terminal points of the axonal arbor at "t". Pairwise distances between the simulated
539 addition or elimination events within a stimulation period was calculated and then the
540 mean pairwise distance for stimulation period obtained. This randomization was repeated
541 100 times and the average simulated mean pairwise distance plotted on **Figure S2**. The
542 ratio of the observed and simulated mean pairwise distance was plotted on **Figure 2E-F**.
543 The imaging experiments and the axonal reconstructions were performed blind to the
544 experimental design, except for one axon in the TrkB-Fc group.
545

546 ## Statistical analysis

547 Aligned rank transform for non-parametric factorial 2-way mixed design model with BDNF
548 manipulation as between-subject and visual stimulation (**Figures 1E-F and 2E-F**) or time
549 (**Figures 3E-G and 4D**) as within-subject factor was performed using ART tool package
550 implemented in R (Wobbrock et al., 2011). After obtaining significant interaction, to
551 assess statistical significance of simple main effects, either Kruskal-Wallis or Friedman's
552 test, followed by pairwise post-hoc tests corrected for multiple comparisons using the
553 Benjamini, Krieger and Yekutieli (BKY) two-stage linear step-up procedure (Benjamini et

554 al., 2006) were carried out using GraphPad Prism 9.0.0 and the results of the tests used
555 for each experiment are described for each figure legend and in supplemental table 1.
556 The axonal reconstructions and their spanning fields in **Figure 4A-C** were plotted using
557 Plotly.

558

559

561

562 **Key Resources Table**

Reagent or Resource	Source	Identifier
Antibodies		
Chicken anti-GFP	Abcam	Cat. no. ab13970, RRID: AB_300798
Rabbit anti-β-tubulin	Santa Cruz	Cat. No. sc-9104, RRID: AB_2241191
Rabbit anti-phospho-Trk	Cell Signalling	Cat. No. 9141, RRID: AB_2298805
Goat anti-rabbit IgG conjugated to horseradish peroxidase	Jackson Immuno Research, Inc.	RRID: AB_2307391
Goat anti-chicken IgG conjugated to horseradish peroxidase	Jackson Immuno Research, Inc.	RRID: AB_2337381
Chemicals, Peptides and Recombinant proteins		
Ctrl-MO-3'lissamine	Gene Tools	N/A
p75-MO-3'lissamine	Gene Tools/ (Je *et al.*, 2012)	N/A
TrkB-MO-3'lissamine	Gene Tools/ (Du and Poo, 2004; Je *et al.*, 2012)	N/A
BDNF	Alomone Labs	Cat. No. B-250
TrkB-Fc (Recombinant Human Chimera)	R&D Systems	Cat. No. 688-TK
Turbocurarine hydrochloride pentahydrate	Sigma	Cat. T2379
Human chorionic gonadotropin	Sigma	Cat. No. CG10-10vl
Pregnant mare's serum gonadotropin	Prospec	Cat No. HOR-272
Halt™ protease/phosphatase inhibitor cocktail	ThermoScientific	Cat. No. P178442
MS-222	Sigma	Cat. No. A5040
UltraPureTM Low Melting Point Agarose	Invitrogen	Cat. No. 16520

Experimental Models: Organisms/Strains		
Albino *Xenopus laevis*	Nasco	RRID: XEP_Xla300
Recombinant DNA		
Plasmid: pEGFP-N1	Clonetech	Cat. No. 6085-1
Plasmid: p75-EGFP	This paper	N/A
Plasmid: MOres-p75-EGFP	This paper	N/A
Software and Algorithms		
Imaris 6.4.2 and 9.5.1	Bitplane	N/A
CANDLE	(Coupé *et al.*, 2012)	N/A
Fiji	(Schindelin *et al.*, 2012)	N/A
Trees Toolbox	(Cuntz *et al.*, 2010) https://www.treestoolbox.org/	N/A
PyImarisSWC	Sarun Gulyanon	N/A
Dynamo	Kurt Haas (UBC)	N/A
ARTool Package for R	(Wobbrock *et al.*, 2011)	N/A
GraphPad Prism 9.0.0	GraphPad	N/A
Plotly	https://plotly.com/python/3d-mesh/	N/A

566 ## Figures and legends

567 **Figure 1. Blocking distinct components of BDNF signaling differentially affects**
568 **correlation-dependent branch dynamics**

569 (A) Retinal co-electroporation of EGFP and MO to label ipsi axons with receptor knock-
570 down. Two-photon z-series projection of ipsi axon with EGFP (cyan) and lissamine-
571 tagged Ctrl-MO (magenta). For TrkB-Fc experiments, intraventricular injection was
572 performed >1 h prior to imaging. (B) Visual stimulation (10 ms light flash; 0.5 Hz) delivered
573 via optic fibers positioned by the tadpoles' eyes. Ipsi axons were imaged every 10 min: 1
574 h Darkness, 1.5 h or 2 h Asynchronous, 1.5 h or 2h Synchronous stimulation (DAS:
575 shorter protocol used for intraventricular TrkB-Fc) (C) Reconstructed arbors showing
576 added, lost and transient branches. Drawings summarize branch dynamics over 1 h.
577 Timecourse of branch (D) additions and (E) losses normalized to the average in darkness,
578 DAS (1 h, 1.5 h, 1.5 h). Average branch (F) addition and (G) loss rates per first hour of
579 stimulation. Significant interactions in the two-way mixed design model: (F) $p = 0.02347$;
580 (G) $p = 0.00149$. (within-subject factor: stimulation; between-subject factor: BDNF
581 manipulation); Post-hoc tests corrected for multiple comparisons (BKY two-stage linear
582 step-up procedure): $^{*}p \leq 0.05$, $^{**}p \leq 0.01$. Graphs show (D-E) mean ± s.e.m. and (F-G)
583 median and individual data points. Scale bars: (A) 20 µm; (B) 500 µm.

584

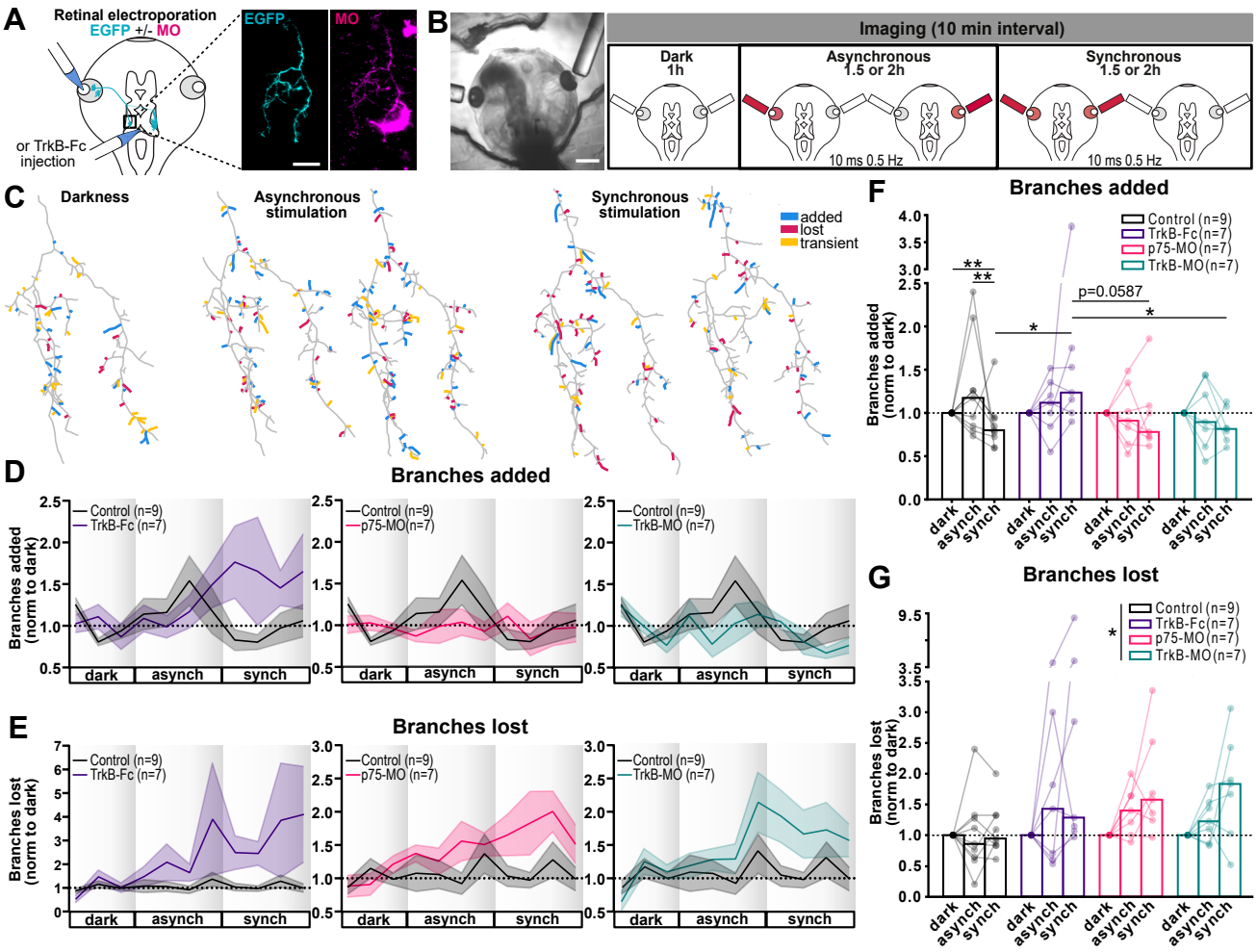
A
Retinal electroporation
EGFP +/- MO
or TrkB-Fc injection
EGFP
MO
B
Imaging (10 min interval)
Dark 1h
Asynchronous 1.5 or 2h
Synchronous 1.5 or 2h
10 ms 0.5 Hz
10 ms 0.5 Hz
C
Darkness
Asynchronous stimulation
Synchronous stimulation
added
lost
transient
D
Branches added
Branches added (norm to dark)
Control (n=9)
TrkB-Fc (n=7)
p75-MO(n=7)
TrkB-MO (n=7)
dark
asynch
synch
E
Branches lost
Branches lost (norm to dark)
F
Branches added
Control (n=9)
TrkB-Fc(n=7)
p75-MO(n=7)
TrkB-MO(n=7)
p=0.0587
G
Branches lost

Figure 1

585

586 **Figure 2. Role of BDNF signaling in local axonal branch elimination induced by**
587 **synchronous stimulation.**

588 (A) Three consecutive reconstructed arbors from a control ipsi axon during synchronous
589 stimulation. Addition and elimination events (for timepoint "*t*") are defined as the
590 coordinates of the branch point of the newly added axonal branch (≥ 1.5 μm) between *t-*
591 *10 min* and *t* (blue), or terminal point of a lost branch between *t* and *t+10 min* (magenta),
592 respectively. (B) All elimination events during DAS (1 h, 1.5 h, 1.5 h) are superimposed
593 on the reconstructed arbor (last timepoint of each stimulation period). (C) Illustration of
594 distances between an elimination event and all the other events (pair distances). (D) All
595 the elimination event pair distances for the axon from (B). Means are denoted as yellow
596 crosses. Normalized branch (E) elimination and (F) addition event pair distances. To
597 correct for changes in arbor size, each point represents the ratio of observed-to-
598 randomized (**Figure S2**) mean event pair distances, normalized to darkness for each
599 axon. Significant interaction in the two-way mixed design model: (E) $p<0.001$; Post-hoc
600 tests corrected for multiple comparisons (BKY two-stage linear step-up procedure): $^*p \leq$
601 0.05, $\ddagger p \leq 0.05$ compared to control. Bars represent median.

602

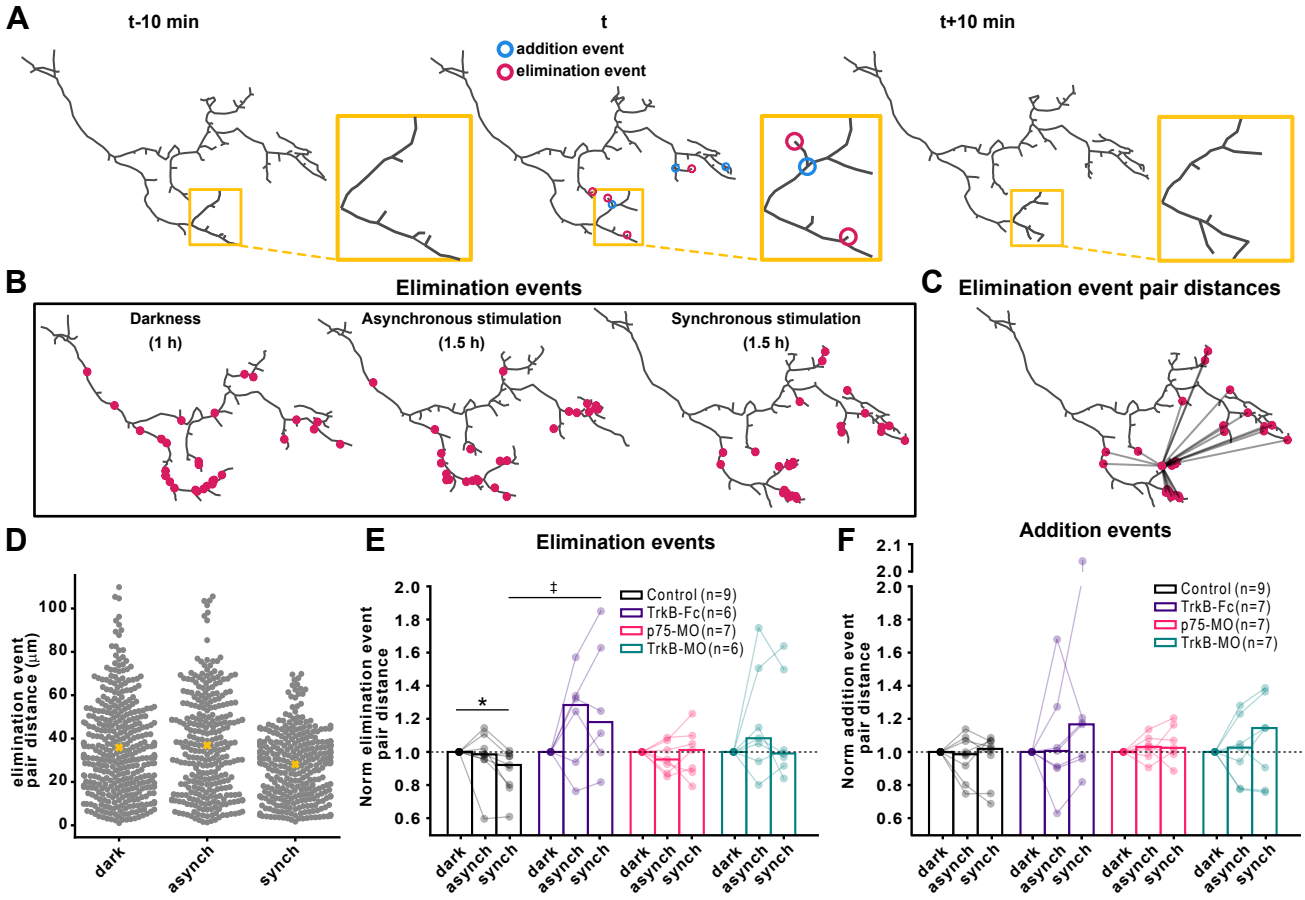
A
t-10 min
t
t+10 min
addition event
elimination event
B
Elimination events
Darkness
(1 h)
Asynchronous stimulation
(1.5 h)
Synchronous stimulation
(1.5 h)
C
Elimination event pair distances
D
elimination event pair distance (µm)
dark
asynch
synch
E
Elimination events
Norm elimination event pair distance
Control (n=9)
TrkB-Fc(n=6)
p75-MO(n=7)
TrkB-MO(n=6)
F
Addition events
Norm addition event pair distance
Control (n=9)
TrkB-Fc(n=7)
p75-MO(n=7)
TrkB-MO(n=7)

Figure 2

603

604 **Figure 3. Effects of retinal TrkB-MO and p75-MO on RGC axonal arbor elaboration**
605 **over days**

606 (A-C) Two-photon Z-series projections over 4 d for example axons co-electroporated with
607 EGFP and (A) Ctrl-MO, (B) p75-MO, (C) TrkB-MO. (D) Reconstructed control arbor from
608 day *4* showing axonal skeleton (black), terminal segments (blue) and terminal points
609 (orange). (E-F) Morphometric analysis including (E) number of terminal points and (F)
610 skeleton length, normalized to day 1. (G) Distribution of terminal segments (percent of
611 total per axon) binned by length. Significant interactions in the two-way mixed design
612 model: (E-F) $p < 0.001$; (G) $p = 0.04394$ (<5 μm bin); $p = 0.01981$ (5-10 μm bin). Post-hoc
613 tests corrected for multiple comparisons (BKY two-stage linear step-up procedure): (E-F)
614 *$p \leq 0.05$, **$p \leq 0.01$ and (G) comparison between day 1 and day 4, (G) comparison
615 between day 2 and day 4: #$p \leq 0.05$, ##$p \leq 0.01$, ###$p \leq 0.001$, (G) comparison between
616 day 3 and day 4: ‡$p \leq 0.05$, ‡‡$p \leq 0.01$. Data represent (E-F) median and individual data
617 points, and (G) median ± iqr. Scale bar: 20 μm applies to all images.

618

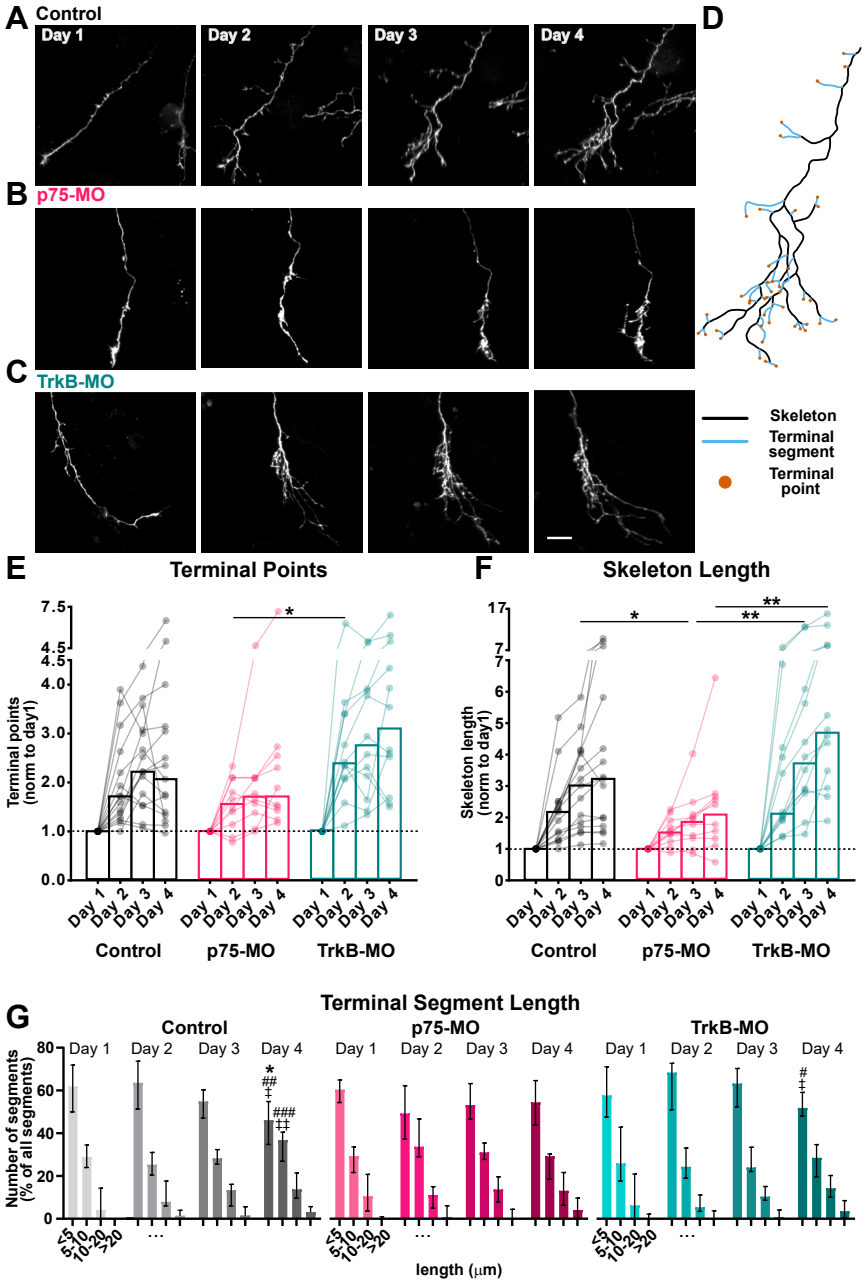
A
Control
Day 1
Day 2
Day 3
Day 4
B
p75-MO
C
TrkB-MO
D
Skeleton
Terminal segment
Terminal point
E
Terminal Points
Terminal points (norm to day1)
Control
p75-MO
TrkB-MO
F
Skeleton Length
Skeleton length (norm to day1)
G
Terminal Segment Length
Number of segments (% of all segments)
length (µm)

Figure 3

619

620 **Figure 4. Opposing effects of retinal TrkB-MO and p75-MO on RGC axon arbor span**
621 **compactness**

622 (A-C) Three-dimensional spans of reconstructed RGC axon arbors over 4 days, co-
623 electroporated with EGFP and MO: (A) Ctrl-MO, (B) p75-MO, and (C) TrkB-MO. (D)
624 Significant interaction in the two-way mixed design model: **p =0.00119. (E) TrkB-MO
625 leads to a faster increase in arbor spanning field volume compared to p75-MO [Arbor
626 spanning field expansion index = (day 4 - day 1)/(day 1 + day 4)], analyzed by Kruskal-
627 Wallis test, p = 0.0175 and pairwise post-hoc tests corrected for multiple comparisons:
628 **p ≤ 0.01. Data represent (D) median and individual points, and (E) median ± iqr. (F)
629 Summary schematic of structural remodeling of an RGC axon instructed by patterned
630 activity: correlated firing (left) and non-correlated firing (right) of axon with neighboring
631 inputs and postsynaptic partner. Zoom-in of proposed molecular and cellular mechanisms
632 underlying (G) Stentian and (H) Hebbian structural plasticity in the developing visual
633 system.

634

635

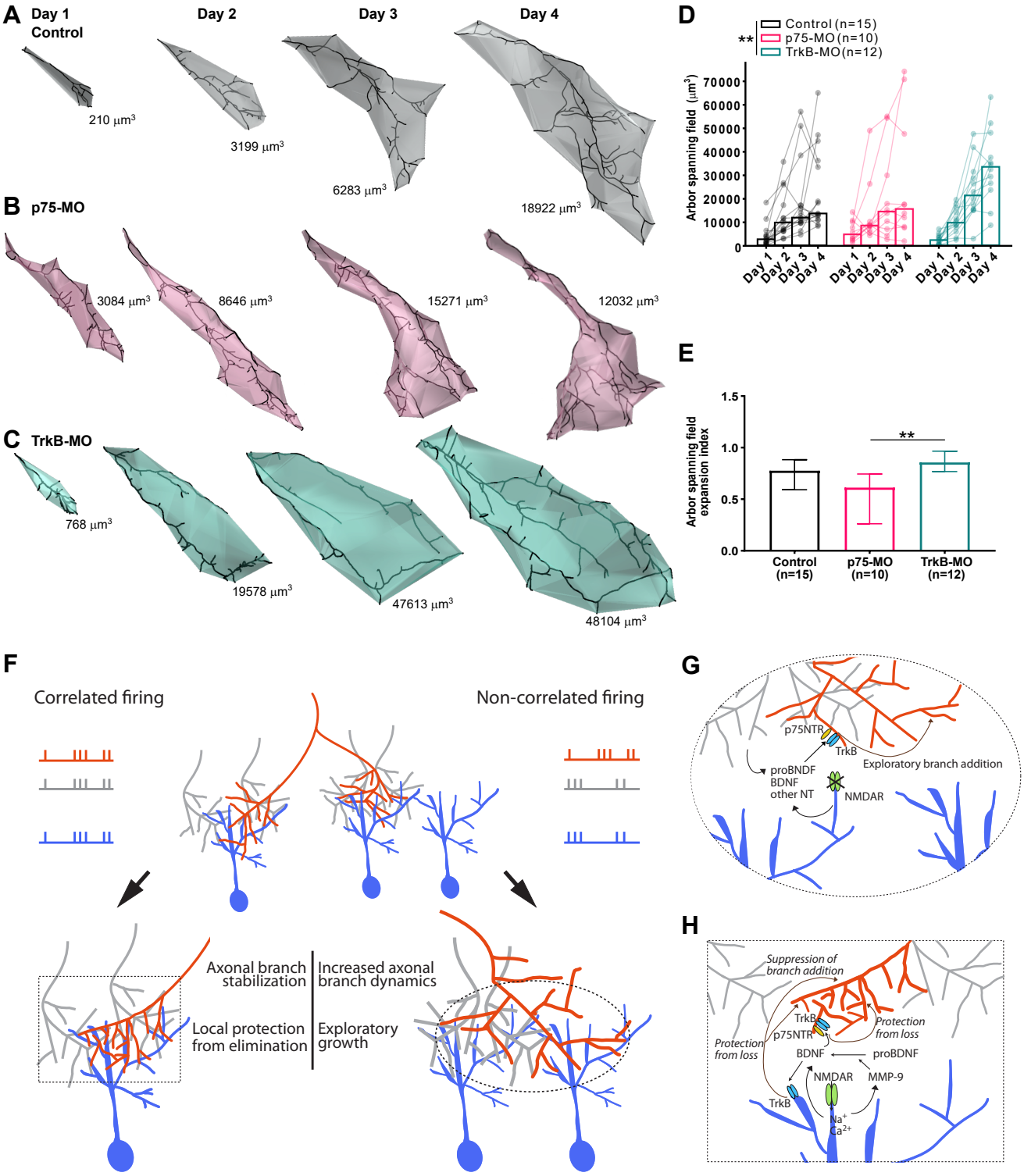
A
Day 1
Control
Day 2
Day 3
Day 4
210 μm³
3199 μm³
6283 μm³
18922 μm³
B
p75-MO
3084 μm³
8646 μm³
15271 μm³
12032 μm³
C
TrkB-MO
768 μm³
19578 μm³
47613 μm³
48104 μm³
D
Control (n=15)
p75-MO (n=10)
TrkB-MO (n=12)
**
Arbor spanning field (μm³)
70000
60000
50000
40000
30000
20000
10000
0
Day 1
Day 2
Day 3
Day 4
E
Arbor spanning field expansion index
1.5
1.0
0.5
0.0
**
Control (n=15)
p75-MO (n=10)
TrkB-MO (n=12)
F
Correlated firing
Non-correlated firing
Axonal branch stabilization
Increased axonal branch dynamics
Local protection from elimination
Exploratory growth
G
p75NTR
TrkB
Exploratory branch addition
proBNDF
BDNF
other NT
NMDAR
H
Suppression of branch addition
TrkB
p75NTR
Protection from loss
Protection from loss
BDNF
proBDNF
NMDAR
MMP-9
TrkB
Na+
Ca2+

Figure 4

636 **Supplemental figures**

637

638 **Figure S1, related to Figure 1: Validation of p75-MO and TrkB-MO**

639 (A) Schematic of the mRNA constructs encoding p75^{NTR}-EGFP fusion protein. Binding of
640 p75-MO to the *p75^{NTR}*-5'UTR-containing mRNA (p75-EGFP mRNA; left) impedes mRNA
641 translation, whereas the inability of p75-MO to bind the construct lacking the *p75^{NTR}*
642 5'UTR (MO-resistant p75-EGFP mRNA; right) spares mRNA translation. (B) Schematic
643 of mRNA construct and MO injection at 2-cell stage, raising injected embryos to stage 26
644 and preparation of whole-animal homogenates. (C) Western blot analysis of
645 homogenates derived from animals injected with combination of p75-EGFP mRNA or
646 MO-resistant p75-EGFP mRNA and p75-MO probed for EGFP and β-tubulin. (D)
647 Schematic of MO injection at 2-cell stage, followed by intraventricular injection of BDNF
648 in morphant tadpoles at stage 46, 1 h before brain homogenate preparation. (E) Western
649 blot analysis of brain homogenates probed for phospho-Trk (p-Trk) and β-tubulin.
650 Approximate size (kDa) is shown next to the bands

651

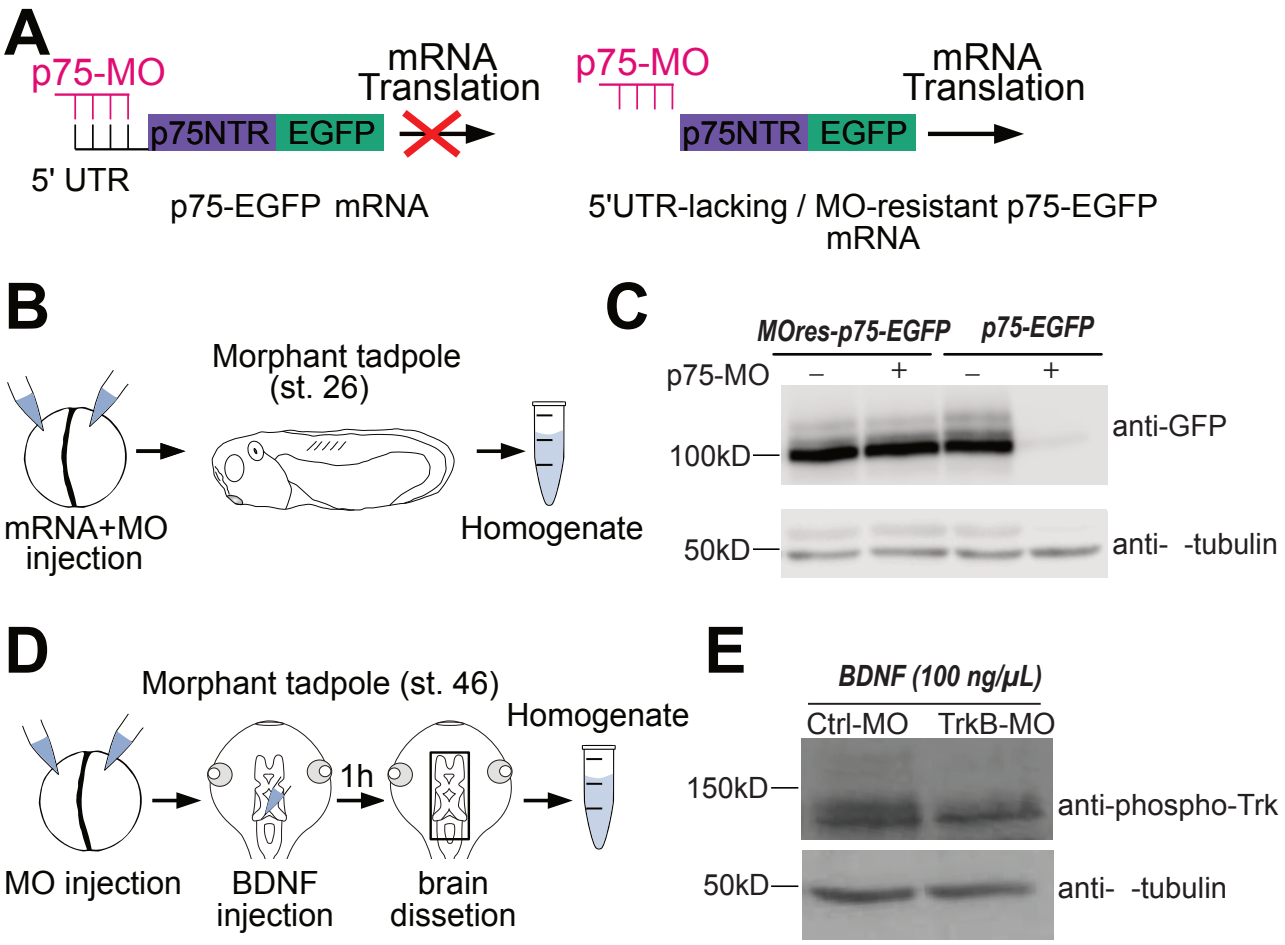

Supplemental Figure 1

Figure S2, related to Figure 2: Monte Carlo simulation of addition and elimination event pair distances

Mean simulated (A) elimination and (B) addition event pair distances in DAS (1 h, 1.5 h, 1.5 h) by redistribution of events at random within the reconstructed arbor. Data represent median and individual data points. Significant interaction in the two-way mixed design model: (A) $p = 0.0024611$; (B) $p<0.001$. Pairwise post-hoc tests corrected for multiple comparisons (BKY two-stage linear step-up procedure): *$p \leq 0.05$, **$p \leq 0.01$, ‡$p \leq 0.05$, compared to control.

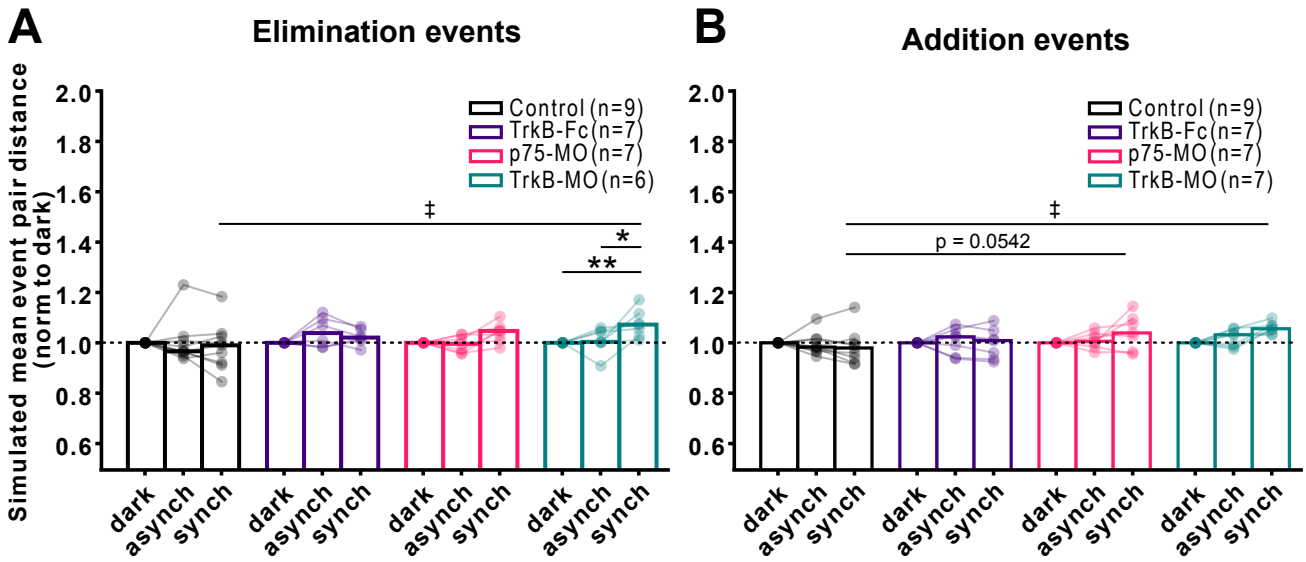

Supplemental Figure 2

664 Supplemental Table 1

Figure	F-statistic (interaction)	Friedman statistic	Kruskal-Wallis statistic
1E	F(6,52) = 2.69767	Control: 8.222 TrkB-Fc: 3.308 p75-MO: 0.6667 TrkB-MO: 1.556	asynch: 1.219 synch: 8.867
1F	F(6,52) = 2.9478	Control: 0.4000 TrkB-Fc: 3.714 p75-MO: 4.667 TrkB-MO: 4.571	asynch: 3.096 synch: 6.122
2E	F(6,50) = 4.9704	Control: 6.889 TrkB-Fc: 1.333 p75-MO: 1.143 TrkB-MO: 0.8571	asynch: 4.962 synch: 6.845
2F	F(6,52) = 1.7576	–	–
3E	F(6,102) = 4.5683	Control: 25.07 p75-MO: 17.59 TrkB-MO: 23.70	Day 2: 7.969 Day 3: 5.461 Day 4: 4.605
3F	F(6,102) = 9.2118	Control: 41.00 p75-MO: 14.76 TrkB-MO: 34.90	Day 2: 5.835 Day 3: 9.242 Day 4: 9.984
3G: bin1 (0-5 μm)	F(6,102) = 2.25385	Control: 11.05 p75-MO: 1.848 TrkB-MO: 7.300	Day 1: 0.1906 Day 2: 5.197 Day 3: 1.736 Day 4: 3.183
3G: bin2 (5-10 μm)	F(6,102) = 2.6495	Control: 14.28 p75-MO: 6.152 TrkB-MO: 0.9000	Day 1: 0.4411 Day 2: 6.627 Day 3: 2.343 Day 4: 6.571
3G: bin3 (10-20 μm)	F(6,102) = 0.96009	–	–
3G: bin4 (>20 μm)	F(6,102) = 0.442131	–	–
4D	F(6,102) = 4.0146	Control: 28.52 p75-MO: 6.360 TrkB-MO: 32.70	Day1: 4.595 Day 2: 0.07752 Day 3: 2.683 Day 4: 3.072
4E	–	–	8.086
S1A	F(6,50) = 3.9850	Control: 1.556 TrkB-Fc: 2.333 p75-MO: 5.429 TrkB-MO: 12.29	asynch: 4.159 synch: 8.432
S1B	F(6,52) = 5.4860	Control: 3.556 TrkB-Fc: 2.000 p75-MO: 2.000 TrkB-MO: 6.000	asynch: 2.467 synch: 8.678

665

666 **References**

667 Alsina, B., Vu, T., and Cohen-Cory, S. (2001). Visualizing synapse formation in arborizing
668 optic axons in vivo: dynamics and modulation by BDNF. Nat. Neurosci. *4*, 1093–
669 1101.

670 Arroyo, D.A., and Feller, M.B. (2016). Spatiotemporal Features of Retinal Waves Instruct
671 the Wiring of the Visual Circuitry. Front. Neural Circuits *10*, 54.

672 Baho, E., Chattopadhyaya, B., Lavertu-Jolin, M., Mazziotti, R., Awad, P.N., Chehrazi, P.,
673 Groleau, M., Jahannault-Talignani, C., Vaucher, E., Ango, F., et al. (2019). p75
674 Neurotrophin Receptor Activation Regulates the Timing of the Maturation of Cortical
675 Parvalbumin Interneuron Connectivity and Promotes Juvenile-like Plasticity in Adult
676 Visual Cortex. J. Neurosci. *39*, 4489–4510.

677 Balkowiec, A., and Katz, D.M. (2000). Activity-Dependent Release of Endogenous Brain-
678 Derived Neurotrophic Factor from Primary Sensory Neurons Detected by ELISAIn
679 Situ. J. Neurosci. *20*, 7417–7423.

680 Benjamini, Y., Krieger, A.M., and Yekutieli, D. (2006). Adaptive linear step-up procedures
681 that control the false discovery rate. Biometrika *93*, 491–507.

682 Bird, A.D., and Cuntz, H. (2019). Dissecting Sholl Analysis into Its Functional
683 Components. Cell Rep. *27*, 3081-3096.e5.

684 Bronfman, F.C., and Fainzilber, M. (2004). Multi-tasking by the p75 neurotrophin receptor:
685 sortilin things out? EMBO Rep. *5*, 867–871.

686 Chao, M.V., and Hempstead, B.L. (1995). p75 and Trk: a two-receptor system. Trends
687 Neurosci. *18*, 321–326.

688 Cline, H.T., Debski, E.A., and Constantine-Paton, M. (1987). N-methyl-D-aspartate
689 receptor antagonist desegregates eye-specific stripes. Proc. Natl. Acad. Sci. U. S.
690 A. *84*, 4342–4345.

691 Cohen-Cory, S., and Fraser, S.E. (1995). Effects of brain-derived neurotrophic factor on
692 optic axon branching and remodelling in vivo. Nature *378*, 192–196.

693 Coupé, P., Munz, M., Manjón, J.V., Ruthazer, E.S., and Collins, D.L. (2012). A CANDLE
694 for a deeper in vivo insight. Med. Image Anal. *16*, 849–864.

695 Cuntz, H., Forstner, F., Borst, A., and Häusser, M. (2010). One rule to grow them all: a
696 general theory of neuronal branching and its practical application. PLoS Comput.
697 Biol. *6*.
698 Demas, J.A., Payne, H., and Cline, H.T. (2012). Vision drives correlated activity without
699 patterned spontaneous activity in developing Xenopus retina. Dev. Neurobiol. *72*,
700 537–546.
701 Dieni, S., Matsumoto, T., Dekkers, M., Rauskolb, S., Ionescu, M.S., Deogracias, R.,
702 Gundelfinger, E.D., Kojima, M., Nestel, S., Frotscher, M., et al. (2012). BDNF and
703 its pro-peptide are stored in presynaptic dense core vesicles in brain neurons. J.
704 Cell Biol. *196*, 775–788.
705 Dougherty, K.D., and Milner, T.A. (1999). p75NTR immunoreactivity in the rat dentate
706 gyrus is mostly within presynaptic profiles but is also found in some astrocytic and
707 postsynaptic profiles. J. Comp. Neurol. *407*, 77–91.
708 Du, J.-L., and Poo, M.-M. (2004). Rapid BDNF-induced retrograde synaptic modification
709 in a developing retinotectal system. Nature *429*, 878–883.
710 Dziembowska, M., Milek, J., Janusz, A., Rejmak, E., Romanowska, E., Gorkiewicz, T.,
711 Tiron, A., Bramham, C.R., and Kaczmarek, L. (2012). Activity-dependent local
712 translation of matrix metalloproteinase-9. J. Neurosci. *32*, 14538–14547.
713 Gore, S.V., James, E.J., Huang, L.-C., Park, J.J., Berghella, A., Thompson, A., Cline,
714 H.T., and Aizenman, C. (2021). Role of matrix metalloproteinase-9 in
715 neurodevelopmental disorders and plasticity in Xenopus tadpoles. Elife *10*, e62147.
716 Guo, W., Nagappan, G., and Lu, B. (2018). Differential effects of transient and sustained
717 activation of BDNF-TrkB signaling. Dev. Neurobiol. *78*, 647–659.
718 Haapasalo, A., Sipola, I., Larsson, K., Åkerman, K.E.O., Stoilov, P., Stamm, S., Wong,
719 G., and Castrén, E. (2002). Regulation of TRKB Surface Expression by Brain-
720 derived Neurotrophic Factor and Truncated TRKB Isoforms*. J. Biol. Chem. *277*,
721 43160–43167.
722 Harward, S.C., Hedrick, N.G., Hall, C.E., Parra-Bueno, P., Milner, T.A., Pan, E., Laviv, T.,
723 Hempstead, B.L., Yasuda, R., and McNamara, J.O. (2016). Autocrine BDNF-TrkB
724 signalling within a single dendritic spine. Nature *538*, 99–103.

725 Hebb, D.O. (1949). The Organization of Behavior:A Neuropsychological Theory (New
726 York: John Wiley).
727 Hermey, G., Riedel, I.B., Rezgaoui, M., Westergaard, U.B., Schaller, C., and Hermans-
728 Borgmeyer, I. (2001). SorCS1, a member of the novel sorting receptor family, is
729 localized in somata and dendrites of neurons throughout the murine brain. Neurosci.
730 Lett. *313*, 83–87.
731 Holt, C.E., and Harris, W.A. (1983). Order in the initial retinotectal map in Xenopus: a new
732 technique for labelling growing nerve fibres. Nature *301*, 150–152.
733 Horch, H.W., and Katz, L.C. (2002). BDNF release from single cells elicits local dendritic
734 growth in nearby neurons. Nat. Neurosci. *5*, 1177–1184.
735 Hu, B., Nikolakopoulou, A.M., and Cohen-Cory, S. (2005). BDNF stabilizes synapses and
736 maintains the structural complexity of optic axons in vivo. Development *132*, 4285–
737 4298.
738 Je, H.S., Yang, F., Ji, Y., Nagappan, G., Hempstead, B.L., and Lu, B. (2012). Role of pro-
739 brain-derived neurotrophic factor (proBDNF) to mature BDNF conversion in activity-
740 dependent competition at developing neuromuscular synapses. Proc. Natl. Acad.
741 Sci. U. S. A. *109*, 15924–15929.
742 Je, H.S., Yang, F., Ji, Y., Potluri, S., Fu, X.-Q., Luo, Z.-G., Nagappan, G., Chan, J.P.,
743 Hempstead, B., Son, Y.-J., et al. (2013). ProBDNF and mature BDNF as punishment
744 and reward signals for synapse elimination at mouse neuromuscular junctions. J.
745 Neurosci. *33*, 9957–9962.
746 Ji, Y., Lu, Y., Yang, F., Shen, W., Tang, T.T.-T., Feng, L., Duan, S., and Lu, B. (2010).
747 Acute and gradual increases in BDNF concentration elicit distinct signaling and
748 functions in neurons. Nat. Neurosci. *13*, 302–309.
749 Kesner, P., Schohl, A., Warren, E.C., Ma, F., and Ruthazer, E.S. (2020). Postsynaptic
750 and Presynaptic NMDARs Have Distinct Roles in Visual Circuit Development. Cell
751 Rep. *32*, 107955.
752 Kirchner, J.H., and Gjorgjieva, J. (2021). Emergence of local and global synaptic
753 organization on cortical dendrites. Nat. Commun. *12*, 1–18.
754 Kohara, K., Yasuda, H., Huang, Y., Adachi, N., Sohya, K., and Tsumoto, T. (2007). A
755 local reduction in cortical GABAergic synapses after a loss of endogenous brain-

756 derived neurotrophic factor, as revealed by single-cell gene knock-out method. J.
757 Neurosci. *27*, 7234–7244.
758 Kutsarova, E., Munz, M., and Ruthazer, E.S. (2016). Rules for Shaping Neural
759 Connections in the Developing Brain. Front. Neural Circuits *10*, 111.
760 Li, V.J., Schohl, A., and Ruthazer, E.S. (2022). Topographic map formation and the
761 effects of NMDA receptor blockade in the developing visual system. Proc. Natl.
762 Acad. Sci. U. S. A. *119*.
763 López-Bendito, G., and Molnár, Z. (2003). Thalamocortical development: how are we
764 going to get there? Nat. Rev. Neurosci. *4*, 276–289.
765 Marshak, S., Nikolakopoulou, A.M., Dirks, R., Martens, G.J., and Cohen-Cory, S. (2007).
766 Cell-autonomous TrkB signaling in presynaptic retinal ganglion cells mediates axon
767 arbor growth and synapse maturation during the establishment of retinotectal
768 synaptic connectivity. J. Neurosci. *27*, 2444–2456.
769 McLaughlin, T., Hindges, R., and O'Leary, D.D.M. (2003). Regulation of axial patterning
770 of the retina and its topographic mapping in the brain. Curr. Opin. Neurobiol. *13*, 57–
771 69.
772 Mowla, S.J., Pareek, S., Farhadi, H.F., Petrecca, K., Fawcett, J.P., Seidah, N.G., Morris,
773 S.J., Sossin, W.S., and Murphy, R.A. (1999). Differential sorting of nerve growth
774 factor and brain-derived neurotrophic factor in hippocampal neurons. J. Neurosci.
775 *19*, 2069–2080.
776 Mu, Y., and Poo, M.-M. (2006). Spike timing-dependent LTP/LTD mediates visual
777 experience-dependent plasticity in a developing retinotectal system. Neuron *50*,
778 115–125.
779 Munz, M., Gobert, D., Schohl, A., Poquérusse, J., Podgorski, K., Spratt, P., and Ruthazer,
780 E.S. (2014). Rapid Hebbian axonal remodeling mediated by visual stimulation.
781 Science *344*, 904–909.
782 Niculescu, D., Michaelsen-Preusse, K., Güner, Ü., van Dorland, R., Wierenga, C.J., and
783 Lohmann, C. (2018). A BDNF-Mediated Push-Pull Plasticity Mechanism for
784 Synaptic Clustering. Cell Rep. *24*, 2063–2074.

785 Nieuwkoop, P.D. and Faber, J. 1994 (1994). Normal table of Xenopus laevis (Daudin): a
786 systematical and chronological survey of the development from the fertilized egg till
787 the end of metamorphosis. (New York: Garland Pub.).
788 Ohba, S., Ikeda, T., Ikegaya, Y., Nishiyama, N., Matsuki, N., and Yamada, M.K. (2005).
789 BDNF locally potentiates GABAergic presynaptic machineries: target-selective
790 circuit inhibition. Cereb. Cortex *15*, 291–298.
791 Orefice, L.L., Shih, C.-C., Xu, H., Waterhouse, E.G., and Xu, B. (2016). Control of spine
792 maturation and pruning through proBDNF synthesized and released in dendrites.
793 Mol. Cell. Neurosci. *71*, 66–79.
794 Pang, P.T., Teng, H.K., Zaitsev, E., Woo, N.T., Sakata, K., Zhen, S., Teng, K.K., Yung,
795 W.-H., Hempstead, B.L., and Lu, B. (2004). Cleavage of proBDNF by tPA/plasmin
796 is essential for long-term hippocampal plasticity. Science *306*, 487–491.
797 Pratt, K.G., Hiramoto, M., and Cline, H.T. (2016). An Evolutionarily Conserved
798 Mechanism for Activity-Dependent Visual Circuit Development. Front. Neural
799 Circuits *10*, 79.
800 Qian, Z., Gilbert, M.E., Colicos, M.A., Kandel, E.R., and Kuhl, D. (1993). Tissue-
801 plasminogen activator is induced as an immediate-early gene during seizure,
802 kindling and long-term potentiation. Nature *361*, 453–457.
803 Rahman, T.N., Munz, M., Kutsarova, E., Bilash, O.M., and Ruthazer, E.S. (2020).
804 Stentian structural plasticity in the developing visual system. Proc. Natl. Acad. Sci.
805 U. S. A. *117*, 10636–10638.
806 Rajan, I., Witte, S., and Cline, H.T. (1999). NMDA receptor activity stabilizes presynaptic
807 retinotectal axons and postsynaptic optic tectal cell dendrites in vivo. J. Neurobiol.
808 *38*, 357–368.
809 Rösch, H., Schweigreiter, R., Bonhoeffer, T., Barde, Y.-A., and Korte, M. (2005). The
810 neurotrophin receptor p75NTR modulates long-term depression and regulates the
811 expression of AMPA receptor subunits in the hippocampus. Proc. Natl. Acad. Sci.
812 U. S. A. *102*, 7362–7367.
813 Ruthazer, E.S., Akerman, C.J., and Cline, H.T. (2003). Control of axon branch dynamics
814 by correlated activity in vivo. Science *301*, 66–70.

815 Schwartz, N., Schohl, A., and Ruthazer, E.S. (2011). Activity-dependent transcription of
816 BDNF enhances visual acuity during development. Neuron *70*, 455–467.
817 Stent, G.S. (1973). A physiological mechanism for Hebb's postulate of learning. Proc.
818 Natl. Acad. Sci. U. S. A. *70*, 997–1001.
819 Strahler, A.N. (1957). Quantitative analysis of watershed geomorphology. Trans. Engl.
820 Ceram. Circle *38*, 913.
821 Uylings, H.B., Smit, G.J., and Veltman, W.A. (1975). Ordering methods in quantitative
822 analysis of branching structures of dendritic trees. Adv. Neurol. *12*, 347–354.
823 Vignoli, B., Battistini, G., Melani, R., Blum, R., Santi, S., Berardi, N., and Canossa, M.
824 (2016). Peri-Synaptic Glia Recycles Brain-Derived Neurotrophic Factor for LTP
825 Stabilization and Memory Retention. Neuron *92*, 873–887.
826 Vormberg, A., Effenberger, F., Muellerleile, J., and Cuntz, H. (2017). Universal features
827 of dendrites through centripetal branch ordering. PLoS Comput. Biol. *13*, e1005615.
828 Wang, X., Chun, S.-J., Treloar, H., Vartanian, T., Greer, C.A., and Strittmatter, S.M.
829 (2002). Localization of Nogo-A and Nogo-66 receptor proteins at sites of axon-
830 myelin and synaptic contact. J. Neurosci. *22*, 5505–5515.
831 Winnubst, J., Cheyne, J.E., Niculescu, D., and Lohmann, C. (2015). Spontaneous Activity
832 Drives Local Synaptic Plasticity In Vivo. Neuron *87*, 399–410.
833 Wobbrock, J.O., Findlater, L., Gergle, D., and Higgins, J.J. (2011). The aligned rank
834 transform for nonparametric factorial analyses using only anova procedures. In
835 Proceedings of the SIGCHI Conference on Human Factors in Computing Systems,
836 (New York, NY, USA: Association for Computing Machinery), pp. 143–146.
837 Woo, N.H., Teng, H.K., Siao, C.-J., Chiaruttini, C., Pang, P.T., Milner, T.A., Hempstead,
838 B.L., and Lu, B. (2005). Activation of p75NTR by proBDNF facilitates hippocampal
839 long-term depression. Nat. Neurosci. *8*, 1069–1077.
840 Yang, J., Siao, C.-J., Nagappan, G., Marinic, T., Jing, D., McGrath, K., Chen, Z.-Y., Mark,
841 W., Tessarollo, L., Lee, F.S., et al. (2009). Neuronal release of proBDNF. Nat.
842 Neurosci. *12*, 113–115.
843 Yang, J., Harte-Hargrove, L.C., Siao, C.-J., Marinic, T., Clarke, R., Ma, Q., Jing, D.,
844 Lafrancois, J.J., Bath, K.G., Mark, W., et al. (2014). proBDNF negatively regulates

845 neuronal remodeling, synaptic transmission, and synaptic plasticity in hippocampus.
846 Cell Rep. *7*, 796–806.
847 Zagrebelsky, M., and Korte, M. (2014). Form follows function: BDNF and its involvement
848 in sculpting the function and structure of synapses. Neuropharmacology *76 Pt C*,
849 628–638.
850 Zhang, X.H., and Poo, M.-M. (2002). Localized synaptic potentiation by BDNF requires
851 local protein synthesis in the developing axon. Neuron *36*, 675–688.
852 Zhang, J., Ackman, J.B., Xu, H.-P., and Crair, M.C. (2011). Visual map development
853 depends on the temporal pattern of binocular activity in mice. Nat. Neurosci. *15*,
854 298–307.
855 Zou, D.J., and Cline, H.T. (1996). Expression of constitutively active CaMKII in target
856 tissue modifies presynaptic axon arbor growth. Neuron *16*, 529–539.
857
858